IOPscience iopscience.iop.org

Home Search Collections Journals About Contact us My IOPscience

Enhanced p-type conductivity and band gap narrowing in heavily Al doped NiO thin films deposited by RF magnetron sputtering

This article has been downloaded from IOPscience. Please scroll down to see the full text article.

2009 J. Phys.: Condens. Matter 21 115804

(http://iopscience.iop.org/0953-8984/21/11/115804)

View the table of contents for this issue, or go to the journal homepage for more

Download details:
IP Address: 129.252.86.83
The article was downloaded on 29/05/2010 at 18:39

Please note that terms and conditions apply.

J. Phys.: Condens. Matter **21** (2009) 115804 (7pp) doi:10.1088/0953-8984/21/11/115804

Enhanced p-type conductivity and band gap narrowing in heavily Al doped NiO thin films deposited by RF magnetron sputtering

S Nandy[1], U N Maiti[1], C K Ghosh[1] and K K Chattopadhyay[1,2,3]

[1] Thin Film and Nanoscience Laboratory, Department of Physics, Jadavpur University, Kolkata-700032, India
[2] Center for Nanoscience and Technology, Jadavpur University, Kolkata-700032, India

E-mail: kalyan_chattopadhyay@yahoo.com

Received 16 August 2008, in final form 2 February 2009
Published 24 February 2009
Online at stacks.iop.org/JPhysCM/21/115804

Abstract
Stoichiometric NiO, a Mott–Hubbard insulator at room temperature, shows p-type electrical conduction due to the introduction of Ni^{2+} vacancies (V''_{Ni}) and self-doping of Ni^{3+} ions in the presence of excess oxygen. The electrical conductivity of this important material is low and not sufficient for active device fabrication. Al doped NiO thin films were synthesized by radio frequency (RF) magnetron sputtering on glass substrates at a substrate temperature of 250 °C in an oxygen + argon atmosphere in order to enhance the p-type electrical conductivity. X-ray diffraction studies confirmed the correct phase formation and also oriented growth of NiO thin films. Al doping was confirmed by x-ray photoelectron spectroscopic studies. The structural, electrical and optical properties of the films were investigated as a function of Al doping (0–4 wt%) in the target. The room temperature electrical conductivity increased from 0.01–0.32 S cm $^{-1}$ for 0–4% Al doping. With increasing Al doping, above the Mott critical carrier density, energy band gap shrinkage was observed. This was explained by the shift of the band edges due to the existence of exchange and correlation energies amongst the electron–electron and hole–hole systems and also by the interaction between the impurity quasi-particle system.

1. Introduction

The mechanism of electrical conduction in transition-metal oxides such as CoO, NiO and α-Fe_2O_3 has been the subject of extensive investigations for a long time. According to conventional band theory, which is based on the one-electron approximation, transition-metal oxides such as NiO and CoO have a partially filled metal 3d band and therefore should show metallic conductivity. But because of the large separation between the cations, overlapping between the d orbitals is not possible in these structures and hence these compounds in pure stoichiometric form show insulating behavior. Following these phenomena Mott, Hubbard and others established the notion of localization of d electrons and proposed the idea of Mott insulators [1]. According to Verwey and de Boer [2, 3], the occurrence of electrical conduction, for example in NiO, is associated with the presence of Ni ions with different valences at normal lattice sites. This situation can be easily obtained by employing the method of 'controlled valency' [4]. Therefore the introduction of different valency ions (for example Ni^{2+} and Ni^{3+} in NiO) makes the material non-stoichiometric (by increasing the non-metallic character for p-type and metallic character for n-type) and thereby conducting. The electrical conductivities of many metal oxide semiconductors have been enhanced by impurity doping such as Al, Ga in ZnO [5, 6], F, In in SnO_2 [7, 8], etc.

Interestingly enough, heavy doping in semiconductors causes a great modification to their band gaps and electronic structure, which has received considerable attention in recent

[3] Author to whom any correspondence should be addressed.

 © 2009 IOP Publishing Ltd Printed in the UK

years both in scientific and engineering fields for theoretical and practical importance [9–11]. From the point of view of applications, the energy gap of a semiconductor is an essential parameter which determines the current–voltage characteristics of a p–n junction and also the energy of electroluminescent recombination radiation. In a heavily doped semiconductor the dopant carriers occupy the energy states near the band edges of the host semiconductor. For the n-type material the majority carriers are electrons at the bottom of the conduction band (CB) and for the p-type they are holes at the top of the valence band (VB). The correlation between the carriers (electrons or holes) and also with impurity ions gives rise to band edge shift, which causes the band gap shrinkage (BGS). There are many theoretical models with experimental support [12–14] to realize this band gap shrinkage.

Nickel oxide is a Mott–Hubbard insulator [15] that crystallizes in a rocksalt structure (i.e. NaCl-type). It is an attractive material for a wide range of applications such as a p-type transparent conducting electrodes [16], spin-valve giant magnetoresistance (GMR) sensors [17–20], electrochromic display devices [21], chemical sensors [22] and thermoelectric devices [23]. Nickel oxide has excellent chemical stability with a wide band gap in the range 3.6–4.0 eV [24]. Various processes were attempted to synthesize NiO thin films including sputtering [25, 26], electron beam evaporation [27, 28], and the sol–gel technique [29], etc. If the NiO films were defect free (i.e. stoichiometric), only Ni^{2+} band states are expected to appear in the spectroscopic measurements. However, Ni^{0} and Ni^{3+} bonding states are expected due to defects in NiO and the presence of Ni_2O_3, which has a different crystal structure (hexagonal structure). This may confirm the existence of the metallic Ni defects and Ni vacancies in the films. In our previous work [30] we reported the explanations of the origin of non-stoichiometry in NiO and its effect on the p-type conductivity. Actually Ni^{2+} vacancies are replaced by two Ni^{3+} ions when treated in excess oxygen atmosphere. However, the highest electrical conductivity achieved was low.

Recently, various theoretical methods for the calculation of the electronic states in NiO, using the low spin density approximation (LSDA), LSDA + U, or GW approximation have appeared in the literature [31, 32]. However, the behavior of NiO as a p-type semiconductor is not yet fully understood. Also, the electronic structure of NiO makes it an interesting candidate for material research. In this paper we have reported the effect of Al doping on the electrical and optical properties of NiO thin films synthesized by the RF magnetron sputtering technique and found some interesting phenomenon such as band gap shrinkage. Since the ionic radii of Ni^{3+} and Al^{3+} are approximately the same, it is expected that Ni^{3+} will be easily replaced by the Al^{3+} ions. Also assuming the carriers (electron or hole gas) to be non-interacting quasi-particles we calculated the correlation and exchange energies in the conduction and valence bands (electron or holes among themselves) as well as the interaction energy between the dopant impurities for explaining the measured band gap shrinkage.

Table 1. RF sputtering conditions.

RF power: 100 W
Base vacuum: 2.1×10^{-7} Torr
Deposition pressure: 4.2×10^{-3} Torr
Sputtering time: 45 min
$[O_2/(Ar + O_2)]$: 11%
Substrate used: glass
Substrate to target distance: 8 cm
Substrate temperature: 523 K
Parameter varied: percentage of Al doping

2. Experimental details

2.1. Target preparation and film synthesis

The targets for the sputtering were fabricated by taking appropriate amounts of NiO (99.99% Merck) and Al powder (99.99% Aldrich) in a stainless steel grooved holder (2″ diameter) and pressing with a hydraulic press at 120 kg cm^{-2}. The obtained pellets were sintered at 450 °C and were used as a target for sputtering. RF sputtering [33] is a widely used technique for the synthesis of thin films. In our experiment the distance between the substrate and the electrode was kept at 8 cm and the target was held at an angle of 45° to the vertical to avoid larger particulate deposition. The substrate holder was rotated at 26 rpm to achieve better uniformity. The chamber was evacuated by a combination of a turbo molecular and a rotary pump to a base pressure of 2.1×10^{-7} Torr. Sputtering was performed at 4.2×10^{-3} Torr in an argon + oxygen atmosphere, maintaining the $[O_2/(Ar + O_2)]$ ratio to 11%. The target was pre-sputtered for 15 min in the argon atmosphere to remove the surface contamination, if any, and then the shutter was displaced to expose the substrates in the plasma. The films were deposited on glass substrates (Blue Star, India). Before placing them into the deposition chamber, the glass substrates were at first cleaned with mild soap solution, then boiled for 30 min in concentrated H_2SO_4 and H_2O_2 solution and finally they were ultrasonically cleaned in acetone for 15 min. A summary of the deposition conditions is shown in table 1. The sputtering was performed at a fixed substrate temperature of 523 K for different percentages of doping.

2.2. Characterization

The deposited films were characterized by x-ray diffraction (XRD, BRUKER D8 ADVANCE, by Cu Kα radiation) measurements. Optical transmission spectra of the films deposited onto glass substrates were measured by an ultraviolet–visible–near infrared (UV–vis–NIR) spectrophotometer (SHIMADZU-UV-3101-PC) in the wavelength range of 300–1200 nm. The Al doping was confirmed by x-ray photoelectron spectroscopic studies (Specs, Germany, with a hemispherical analyzer HSA-3500) using Mg Kα (1253.6 eV) radiation from an x-ray source operated at 10 kV at 17 mA. Thicknesses of the films were measured by cross-sectional images taken from a scanning electron microscope (SEM). The electrical conductivity of the films was studied by the standard four-probe method using a Keithley electrometer (Model 6514) from 300 to 550 K under

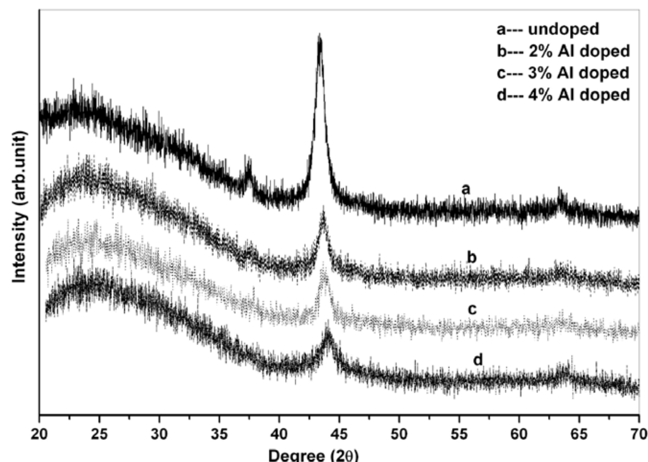

Figure 1. XRD patterns of the NiO thin films for different percentage of Al doping.

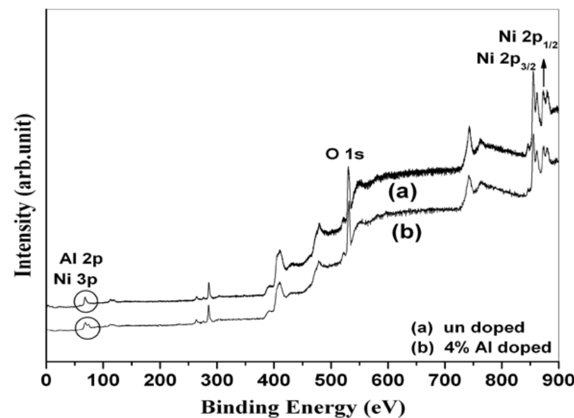

Figure 2. XPS survey scans of the undoped NiO and doped NiO thin film.

vacuum conditions (10^{-3} mbar) to avoid any possible change in composition. The measurement showed linear I–V characteristics over a wide range of applied voltages. Hall measurements were performed at room temperature by a standard set up and the majority carrier concentrations were determined.

3. Results and discussion

3.1. Crystalline structure

3.1.1. XRD analysis. Figure 1 shows the XRD patterns of the nickel oxide (NiO) films deposited on glass substrates with different percentages of Al doping. The peaks could be assigned with the cubic phase of NiO (bunsenite). It is also seen that the film has a (200) preferred orientation and the lattice constants were calculated to be $a_0 = b_0 = c_0 = 4.178$.[4] From the XRD spectra it is also observed that with the increase of Al percentage, the intensity of the peak decreased and its width increased. This indicates that with the increase of Al doping the crystallinity of NiO became poorer and above 6% doping the films becomes amorphous (not shown in the given graph).

3.1.2. XPS analysis. The surface of each film was cleaned by Ar^+ sputtering prior to recording the XPS spectra. Figure 2 shows the XPS survey scan for undoped and Al doped (4%) NiO films. From the observed peaks the binding energies of Ni in NiO were found to be 855 eV (for Ni $2p_{3/2}$), 873 eV (for Ni $2p_{1/2}$), and 68 eV (for Ni 3p) [34]. An O 1s peak in NiO was detected at 530 eV. In the spectra of Al doped NiO we have found a broad peak around 70 eV. A high-resolution scan of this broad peak is shown in figure 3(b). After the Tougard baseline correction, deconvolution of this peak resulted three peaks, at 67.21, 70.06 and 73.46 eV. The peak at 67.21 eV is due to Ni $3p_{3/2}$, at 70.06 eV is due to Ni $3p_{1/2}$ and the peak at 73.46 eV is due to Al 2p. For elemental Al, the Al 2p peak should appear at 72.2 eV [35]; hence the observed shift

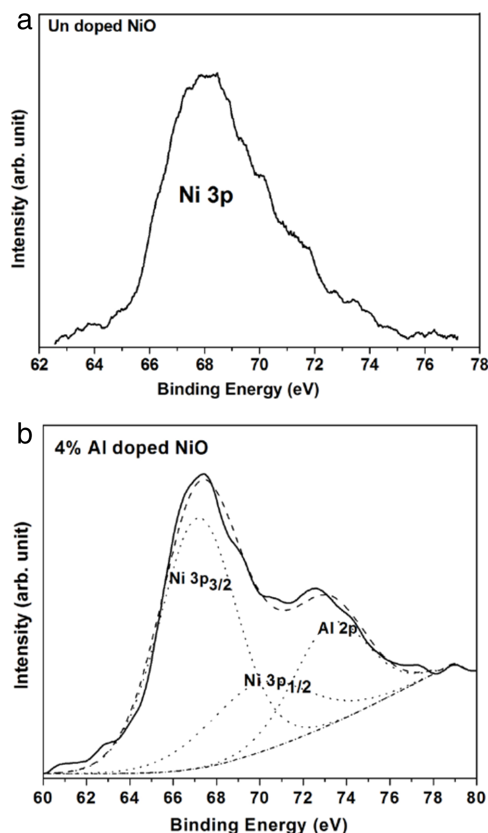

Figure 3. High-resolution core level spectra for undoped and 4% Al doped NiO films showing Ni 3p for undoped and Ni 3p, Al 2p for doped samples.

of binding energy confirmed the doping of Al^{3+} in NiO. In the XPS spectrum of undoped NiO, as shown in figure 3(a), it is seen that the above broad peak is absent and the peak around 68 eV is due to Ni 3p (actually this peak also consists of two peaks due to Ni $3p_{3/2}$ and Ni $3p_{1/2}$; deconvolution not shown in this figure). Table 2 gives the comparison between the nominal percentages of Al in the target and the actual amount of Al doped in NiO thin films estimated from the XPS spectra. It may be mentioned that we also measured the XPS spectra

[4] JCPDS Powder Diffraction File Card 04-0850.

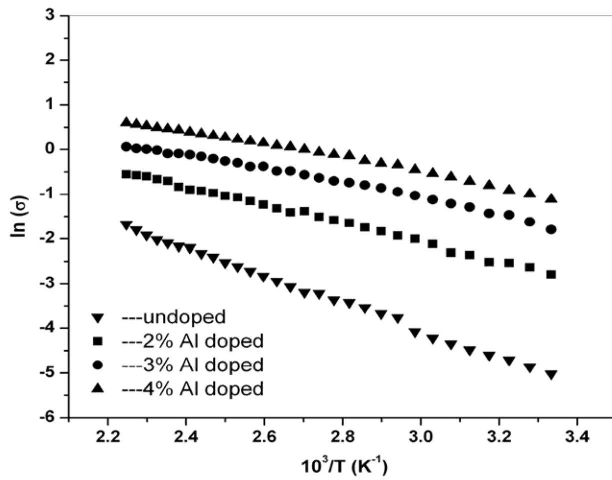

Figure 4. Variation of conductivity with temperature for different NiO thin films on a glass substrate.

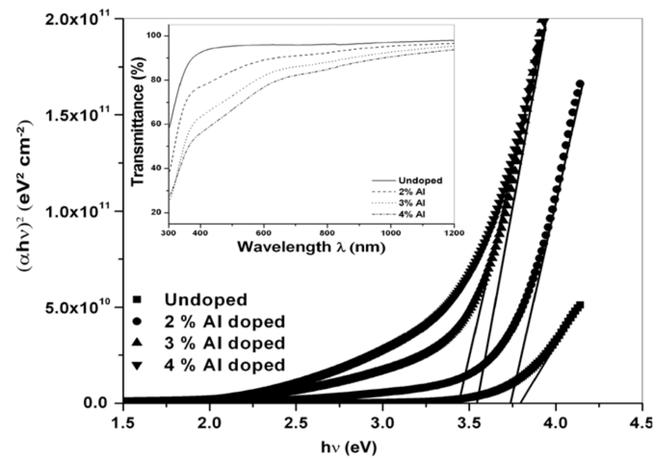

Figure 5. Variation of optical band gap for doped and undoped NiO; inset: optical transmittance spectra of NiO thin film for different doping of Al.

Table 2. Percentage of Al doped in NiO.

Sample name	Nominal % of Al	% of Al from XPS study
NiO 01	Undoped	Undoped
NiO 02	2	1.88
NiO 03	3	2.71
NiO 04	4	3.61

Table 3. Comparison of E_a, σ_{RT} and optical band gap with different % of Al.

Sample	Room temp. conductivity, σ_{RT}(S cm^{-1})	Activation energy, E_a (meV)
Undoped	0.01	262.82
NiO 02	0.06	178.37
NiO 03	0.16	141.32
NiO 04	0.32	132.70

(not shown here) of the target material to find any change in composition from its nominal composition. We found no noticeable change in the nominal composition and the target composition.

3.2. Electrical conductivity measurements

Figure 4 shows the variation of electrical conductivity with temperature for different percentages of Al doping in the NiO films. From the conductivity versus temperature plot we calculated the activation energy of the material by using the following relations:

$$\sigma = \sigma_0 e^{-E_a/kT} \qquad \text{or} \qquad E_a = \{\ln(\sigma_0) - \ln(\sigma)\}kT$$

where σ represents the electrical conductivity, k the Boltzmann constant and E_a is the activation energy. The values of σ_{RT} and the activation energies for different films have been given in table 3. From figure 4 it can also be observed that the electrical conductivity increases with increase in temperature. The reason for the origin of the semiconducting nature is that non-stoichiometric NiO contains many Ni^{2+} vacancies, and to preserve the charge neutrality near the Ni^{2+} vacancies, some of the Ni^{2+} were oxidized to Ni^{3+}. Every δNi^{2+} ion lost from NiO will result in the production of the $2\delta Ni^{3+}$ ions (from Ni_2O_3). The defect chemistry plays an important role in controlling the electrical properties of this material. The overall defect formation equation can be explained as below [36, 37]

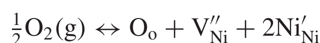

$$\tfrac{1}{2}O_2(g) \leftrightarrow O_o + V''_{Ni} + 2Ni'_{Ni}$$

where V''_{Ni} represents the Ni^{2+} vacancy and the $2Ni''_{Ni}$ act as Ni^{3+} ions. From the above relation it is clear that the defects, Ni^{2+} ion vacancies are the cause for showing the hole conductivity. Thus the mixed valences of Ni (Ni^{2+} in NiO and Ni^{3+} in Ni_2O_3) conform to the non-stoichiometry of NiO. In our previous work [30] we have discussed this mechanism in detail. Here we introduce Al^{3+} ions as the dopant in the NiO film. As the ionic radii of Ni^{3+} and Al^{3+} are very close, so it can easily replace the Ni^{3+} ions in NiO. From the defect chemistry it can be understood that the conductivity of NiO can be varied by varying the Al^{3+} doping percentages. Figure 4 supports this proposition and the highest conductivity achieved was 0.32 S cm^{-1}. The type of the majority carrier was confirmed to be p-type by Hall effect study and the carrier concentrations were determined as mentioned in table 4.

3.3. Optical measurements

Figure 5 shows the band gap variations of NiO with the different percentages of Al doping and the inset shows the corresponding transmittance spectra. The band gap decreases with increasing Al doping in the nickel oxide thin films. It varied from 3.79 eV (for undoped NiO) to 3.43 eV (for maximum Al doped NiO). Table 4 gives the details of band gap variation with increasing percentage of Al doping. We attribute this phenomenon to the effect of free carriers as well as to impurity effects on the band gap. In the following we will explicitly calculate the changes in the band edges of the valence

Table 4. Self-energy terms contributing to the total narrowing ΔE_g and experimental values.

% of Al doped	Carrier concentration n (cm^{-3})	$-\hbar\sum_c$ (eV)	$\hbar\sum_v$ (eV)	$\hbar\sum_v^i$ (eV)	ΔE_g (eV)	Bandgap shift from optical (eV)
2	2.7×10^{17}	0.02	0.027	0.003	0.05	0.06
3	9.6×10^{19}	0.06	0.091	0.069	0.22	0.26
4	3.2×10^{20}	0.07	0.129	0.127	0.33	0.36

and conduction bands using a self-energy technique which takes into account the change in exchange and correlation energy of the appropriate band and the interaction energy due to added free carriers as impurities; by treating all the carriers (electrons and holes) as quasi-free particle.

For a heavily doped semiconductor with carrier concentration above some particular value the electrons occupy the conduction band in the form of an electron gas for n-type materials or a hole gas in the valence band for p-type materials. The energy gap between the conduction band minima and the valence band maxima changes in such cases due to the shift of band edges.

The shift with respect to the unperturbed band gap E_g^0 may be subdivided as [12]

$$\Delta E_g = E_g^0 - E_g = \Delta E_{XC} + \Delta E_I + \Delta E_K.$$

The first term ΔE_{XC} is the exchange and correlation energy, which includes the exchange energy for the holes and electrons in the valence and conduction band respectively and the correlation energy for the electron and hole system. The second term ΔE_I is due to the interaction between the electrons (holes)–impurity ions. The third and last term ΔE_K would be the only contribution excluding the interactions among the electrons, holes and acceptor ions, such as local strain induced by the impurity centers, etc. Here we are only interested in calculating the band edge shift due to Coulomb interactions among the electrons and holes themselves and their interaction with the ionized impurity. The particles can be approximately described as non-interacting quasi-particles [12, 38].

Let the quasi-particle dispersion for the conduction band be

$$E_c(\vec{k}, \omega) = E_c^{(0)}(\vec{k}) + \hbar \sum\nolimits_c(\vec{k}, \omega)$$

where $E_c^{(0)}(\vec{k})$ is the unperturbed band energy and $\hbar\sum_c(\vec{k}, \omega)$ is the self-energy associated with electron–electron scattering.

In the case of the valence band it will be

$$E_\nu(\vec{k}, \omega) = E_\nu^{(0)}(\vec{k}) + \hbar \sum\nolimits_v(\vec{k}, \omega).$$

For heavily doped p-type material, the holes in the valence band can be treated as quasi-free particle. The hole–hole interaction energy, including both exchange and correlation energy, is given by

$$\hbar \sum\nolimits_v(0,0) = \frac{2e^2 k_F}{\varepsilon_S \pi} + \frac{e^2 k_{TF}}{2\varepsilon_S}\left[1 - \frac{4}{\pi}\tan^{-1}\left(\frac{k_F}{k_{TF}}\right)\right].$$

The calculation was carried out in the same fashion, considering electrons as quasi-free particles in the conduction band for a heavily doped n-type material as done by Berggren and Sernelius [12]. For the conduction band in a p-type material, as the electron concentration is very low, we can neglect the exchange term. The correlation energy between the electron–electron interactions can then be

$$\hbar \sum\nolimits_c(0,0) = -\frac{e^2 k_{TF}}{2\varepsilon_S}$$

where k_F, the Fermi wavevector, is given by the relation $k_F = (3\pi^2 n)^{1/3}$ and $k_{TF} = (\frac{2}{\sqrt{\pi}})(\frac{k_F}{a_B})^{1/2}$ is the Thomas–Fermi screening wavevector. Here $a_B = 0.53\varepsilon_S(\frac{m_0}{m^*})$ is the Bohr radius measured in angstrom (Å). Here we take $\varepsilon_S = 12.76$ the static dielectric constant of the NiO [39].

Therefore the total energy contributed by the exchange and correlation energies between the electron–electron, the hole–hole and the electron–hole system is

$$\Delta E_{XC} = \hbar \sum\nolimits_c(0,0) - \hbar \sum\nolimits_v(0,0).$$

The second contribution energy term is due to the interaction between the quasi-particles (holes and electrons) and the impurity ions. Here we can neglect the term electron–impurity interaction, because of very low concentration of electrons in the conduction band. Therefore we only take the impurity–hole interaction energy contribution term, which can approximately be written as

$$\hbar \sum\nolimits_v^{e-i} = \frac{4\pi e^2 n}{\varepsilon_S a_B k_{TF}^3}.$$

Hence,

$$\Delta E_I = \hbar \sum\nolimits_c^i - \hbar \sum\nolimits_v^i \approx -\hbar \sum\nolimits_v^i.$$

The total band gap energy shift is therefore,

$$\Delta E_g = \Delta E_{XC} + \Delta E_I = \hbar \sum\nolimits_c(0,0) - \hbar \sum\nolimits_v(0,0) + \Delta E_I.$$

The calculated energy shift of the conduction band minima and the valence band maxima for the electron–electron and the hole–hole interaction is given in figure 6. From the figure we can observe that the upward shift of VB and downward shift of CB are little different because of the difference between the effective masses of electrons and holes of nickel oxide. Furthermore, at very low doping concentrations impurity scattering has a negligible effect on the band gap narrowing but with the increase of the hole concentration the hole–impurity interaction terms become substantial. A comparison of band gap shift with the carrier concentration is shown in figure 7, where the solid curve represents the theoretical values and the dotted curve represents the corresponding measured optical band gap.

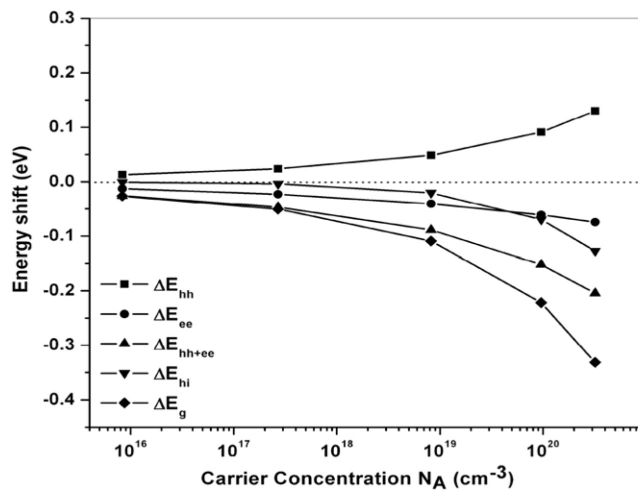

Figure 6. The calculated energy shifts of (i) the conduction band minima, (ii) the valence band maxima, (iii) impurity scattering, (iii) exchange and correlation energy between electron–electron, hole–hole and electron–hole systems and (iv) total band gap shrinkage.

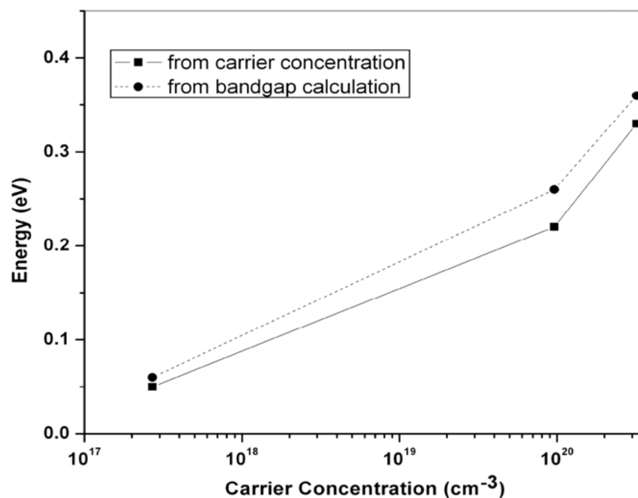

Figure 7. The comparison of band gap energy shift from carrier density and from optical measurements.

4. Conclusion

NiO thin films with (200) preferred orientation on glass substrates were synthesized by RF magnetron sputtering at 523 K substrate temperature using a nickel oxide target with different percentages of Al doping. It was confirmed that with the increase of Al doping the percentage electrical conductivity increased. The conductivity of the undoped NiO was 0.01 S cm^{-1} while it increased up to 0.32 S cm^{-1} for 4% nominal doping of Al in NiO. The type of carrier was confirmed to be p-type by a Hall effect study. Interestingly, with increasing doping concentration in the NiO, a band gap shrinkage of up to 0.36 eV was observed. For undoped NiO the band gap was found to be 3.79 eV while with 4% Al doping it decreased to 3.43 eV. An estimation of the band gap shrinkage was obtained by considering various interactions among the carriers and ion cores. The experimentally measured band gap shrinkage and theoretically obtained values showed good agreement.

Acknowledgment

The authors wish to thank the Department of Science and Technology (DST), the Government of India, for financial support.

References

[1] Tsuda N, Nasu K, Fumitory A and Sartor K 1999–2000 *Electronic Conduction in Oxides* (Berlin: Springer) p 213
[2] Wu K-Y, Wang C-C and Chen D-H 2007 *Nanotechnology* **18** 305604
[3] Kim H, Auyeung R C and Pique A 2008 *Thin Solid Films* **516** 5052
[4] Kim S H, Park N-M, Kim T Y and Sung G Y 2005 *Thin Solid Films* **475** 262
[5] Persson C, Lindefelt U and Sernelius B E 1999 *Phys. Rev.* B **60** 16479
[6] Verwey E J W and de Boer J H 1936 *Rec. Trav. Chim.* **55** 531
[7] de Boer J H and Verwey E J W 1937 *Proc. Phys. Soc.* **49** 59
[8] Verwey E J W 1951 *Semiconducting Materials* (London: Butterworths)
[9] Persson C, Lindefelt U and Sernelius B E 1999 *Phys. Rev.* B **60** 16479
[10] Sernelius B E and Berggren K-F 1981 *Recent Developments in Condensed Matter Physics* vol 3, ed J T Devreese, L F Lemmens, V E Doren and J Van Royen (New York: Plenum)
[11] Wu J, Walukiewicz W, Shan W, Yu K M, Ager J W III, Haller E E, Lu H and Schaff W J 2002 *Phys. Rev.* B **66** 201403
[12] Berggren K-F and Sernelius B E 1981 *Phys. Rev.* B **24** 1971
[13] Inkson J C 1976 *J. Phys. C: Solid State Phys.* **9** 1177
[14] Persson C, Ahuja R and Johansson B 2001 *Phys. Rev.* B **64** 033201
[15] Brandow B H 1997 *Adv. Phys.* **26** 651
[16] Chan I M, Hsu T Y and Hong F C 2002 *Appl. Phys. Lett.* **81** 1899
[17] Carey M J and Berkowitz A E 1993 *J. Appl. Phys.* **73** 6892
[18] Soeya S, Hoshiya H, Meguro K and Fukui H 1997 *Appl. Phys. Lett.* **71** 3424
[19] Hwang D G, Lee S S and Park C M 1998 *Appl. Phys. Lett.* **72** 2162
[20] Koide S 1965 *J. Phys. Soc. Japan* **20** 123
[21] Yoshimura K, Miki T and Tanemura S 1995 *Japan. J. Appl. Phys.* **34** 2440
[22] Hotovy I, Huran J, Siciliano P, Capone S, Spiess L and Rehacek V 1999 *Sensors Actuators* B **57** 147
[23] Shin W and Murayama N 2000 *Mater. Lett.* **45** 302
[24] Swagten H J M, Strijkers G J, Bloemen P J H, Willekens M M H and De Jonge W J M 1996 *Phys. Rev.* B **53** 1039
[25] Nishizawa S, Tsurumi T, Hyodo H, Ishibashi Y, Ohashi N, Yamane M and Fukunaga O 1997 *Thin Solid Films* **302** 133
[26] Yu G H, Zeng L R, Zhu F W, Chai C L and Lai W Y 2001 *J. Appl. Phys.* **90** 4039
[27] Otterman C R, Temmink A and Bange K 1990 *Thin Solid Films* **193/194** 409
[28] Manago T, Ono T, Miyajima H, Yamaguchi I, Kawaguchi K and Sohma M 2000 *Thin Solid Films* **374** 21
[29] Jiao Z, Wu M G, Qin Z and Xu H 2003 *Nanotechnology* **14** 458

[30] Nandy S, Saha B, Mitra M K and Chattopadhyay K K 2007 *J. Mater. Sci.* **42** 5766
[31] Chen X, Wu N J, Smith L and Ignatiev A 2004 *Appl. Phys. Lett.* **84** 14
[32] Terakura K, Williams A R, Oguchi T and Kübler J 1984 *Phys. Rev.* B **40** 4734
[33] Lu Y M, Hwang W S, Yang J S and Chuang H C 2002 *Thin Solid Films* **420/421** 54
[34] Wanger C D, Riggs W M, Davis L E and Moulder JF 1979 *Handbook of X-Ray Photoelectron Spectroscopy* (Eden Prairie, MN: Perkin-Elmer Corporation)
[35] *US Patent Specification* 5650361
[36] Kofstad P 1972 *Non-Stoichiometry, Diffusion, and Electrical Conductivity in Binary Metal Oxidex* (New York: Wiley) p 44
[37] Kingery W D, Bowen H K and Ulhmann D L 1976 *Introduction to Ceramic* 2nd edn (New York: Wiley) p 899
[38] Fetter A L and Walecka J D 1971 *Quantum Theory of Many-Particle Systems* (New York: McGraw-Hill)
[39] Oliver P M, Watson G W and Parker S C 1995 *Phys. Rev.* B **52** 5323